Heliyon 10 (2024) e29273

Contents lists available at ScienceDirect

Heliyon

journal homepage: www.cell.com/heliyon

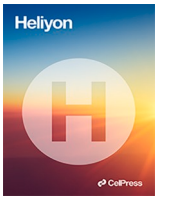

Research article

Cathepsin L promotes oesophageal squamous cell carcinoma development and may be associated with tumour-associated macrophages

Zhenhu Zhang [a,1], Jianyu Wang [a,1], Yamin Shi [b], Ben Wang [c,**], Dong Wang [a,*]

[a] Department of Thoracic Surgery, Shandong Provincial Hospital Affiliated to Shandong First Medical University, Jinan, 250021, China
[b] School of Foreign Languages, Shandong University of Finance and Economics, Jinan, 250014, China
[c] Department of Gastroenterology, Shandong Provincial Hospital Affiliated to Shandong First Medical University, Jinan, 250021, China

ARTICLE INFO

Keywords:
Oesophageal squamous cell carcinoma
Cathepsin L
Tumour-associated macrophages
Immunotherapy
Prognosis

ABSTRACT

Background: Oesophageal squamous cell carcinoma (ESCC) is a leading cause of cancer-related deaths worldwide because existing treatments are often insufficient. Therefore, new, reliable biomarkers must be identified. *CTSL* overexpression is closely associated with tumour progression and poor prognosis. However, the role and mechanism of *CTSL* as an oncogene in ESCC remain unclear.

Methods: Genome-wide association study (GWAS) data were used for Mendelian randomization analysis to investigate the possible relationships between *CTSL* and ESCC. The correlation between *CTSL* expression and prognosis was analysed using GEO, TCGA, and GEPIA data. We compared *CTSL* expression among the cell types using single-cell sequencing. Correlations between *CTSL* and the tumour microenvironment, immune cell infiltration, tumour mutational load, immunological checkpoints, and treatment sensitivity in patients with ESCC were investigated. Finally, using mouse models and cellular investigations, we assessed the effects of *CTSL* on the growth, apoptosis, and metastasis of ESCC tumour cells.

Results: CTSL was overexpressed in ESCC and correlated with prognosis. We also discovered its close association with cell immunity, especially with tumour-associated macrophages and immune checkpoints in the tumour microenvironment. *CTSL* may play a key role in ESCC development by affecting M2 macrophage polarisation. *CTSL* and the M2 macrophage marker genes showed significant positive correlations. Mendelian randomization analysis confirmed a relationship between *CTSL* and ESCC. Finally, our in vitro and in vivo experiments demonstrated that *CTSL* promoted the proliferation and migration of ESCC cells, validating our bioinformatic analysis.

Conclusion: CTSL emerged as a crucial gene in ESCC that influences patient prognosis and immunity, particularly in association with M2 macrophages. Therefore, targeting or modulating CTSL levels may provide new therapeutic strategies for patients with ESCC.

* Corresponding author.
** Corresponding author.
E-mail addresses: wangben@bjmu.edu.cn (B. Wang), sdphwd@163.com (D. Wang).
[1] These authors contributed equally to this work and share first authorship.

https://doi.org/10.1016/j.heliyon.2024.e29273
Received 19 March 2024; Received in revised form 2 April 2024; Accepted 3 April 2024
Available online 6 April 2024

1. Introduction

Oesophageal cancer (EC) ranks sixth worldwide in terms of mortality rate and poses a pressing global health challenge [1]. EC manifests in two forms, oesophageal squamous cell carcinoma (ESCC) and oesophageal adenocarcinoma, with ESCC constituting 90 % of all EC cases [2]. Patients with ESCC experience poor survival rates, and standard treatments combining surgery, radiotherapy, and chemotherapy are often ineffective [3], necessitating the identification of reliable biological markers for the prognosis and treatment of ESCC.

The tumour microenvironment (TME) has a significant impact on tumour development, owing to its ability to suppress the immune system by inhibiting and depleting T, B, and natural killer cells. This action weakens the defense system of the body against tumours, enabling them to evade the immune system [4–7]. Numerous studies have demonstrated an association between multiple resistant cell populations in the TME and development, invasion, and metastasis [8–10]. For instance, the predictive role of tumour-infiltrating lymphocytes in ESCC has been highlighted [11,12].

Various immune cell populations infiltrate the TME, with tumour-associated macrophages (TAMs) being the most prevalent. In addition to their pro-tumourigenicity, TAMs suppress the immune system, promote neoangiogenesis, improve tissue invasion, and facilitate distant metastasis, all of which are crucial for tumour formation [13]. Macrophages are highly plastic and have two main phenotypes, M1 and M2. A recent review of 300 studies found that patients with a higher presence of M2 macrophages tended to have a relatively poor prognosis, whereas the presence of M1 macrophages corresponded to a better prognosis [14]. Most importantly, M2-polarized TAMs can promote tumour growth, angiogenesis, and metastasis, and are associated with malignant progression and poor prognosis in many human cancers. Additionally, patients with high degrees of M2-polarized TAM infiltration often have lower survival rates [15]. Therefore, investigating the infiltration of M2 macrophages in ESCC, particularly the core genes involved in M2 macrophage polarisation, may help develop more effective treatment strategies.

The *CTSL* gene is localised at 9q21.33 and encodes a lysosomal cysteine protease comprising 333 amino acids with a molecular weight of 37,564 Da. The protein primarily functions in the terminal degradation of intracellular and cytosolic proteins [15,16]. *CTSL* upregulation has been widely reported in human malignant tumours, including breast, ovarian, colon, adrenal, bladder, prostate, and thyroid cancers [17]. *CTSL* is associated with cancer progression and metastatic aggressiveness [18]. Notably, targeting *CTSL* by downregulating its expression through RNA interference in different tumour models, including glioma, osteosarcoma, myeloma, and melanoma, has been shown to suppress tumourigenicity and invasiveness [19–22]. However, the specific mechanisms underlying the role of *CTSL* in EC, particularly ESCC, remain unknown.

To gain a deeper understanding of the function of *CTSL* in ESCC, we conducted a comprehensive analysis of *CTSL* expression levels and their correlation with prognosis using the TCGA, GEO, and GEPIA databases. Furthermore, we used the Gene Ontology, Kyoto Encyclopedia of Genes and Genomes, and Gene Set Variation Analysis (GO, KEGG, and GSVA) methods to analyse the relationship between *CTSL* and immune responses. Using single-cell RNA sequencing data validated using the TISCH database, we examined the relationship between *CTSL* and the TME, immune cell infiltration, tumour mutation load, immune checkpoints, and drug sensitivity in patients with ESCC. We explored the relationship between *CTSL* and M2 macrophage polarisation. Additionally, we established a *CTSL*-associated risk model. Mendelian randomization analysis was performed using the GWAS dataset to explore the potential relationship between *CTSL* and EC, and the results were subjected to meta-analysis. Finally, we corroborated the effects of *CTSL* on ESCC through cellular experiments and construction of mouse models to evaluate tumour cell proliferation, apoptosis, and metastasis.

2. Materials and methods

2.1. Data preparation

ESCC expression profiling datasets GSE53624 [23], GSE161533 [24], GSE20347 [25], GSE196756 [26], and GSE188900 [27] were downloaded from the official GEO website (https://www.ncbi.nlm.nih.gov/geo/). Detailed information on these datasets is provided in Table S1. The GEPIA database (http://gepia.cancer-pku.cn/) was used for additional validation. Transcripts per million expression profiling data and survival data of 93 patients with ESCC who underwent gene sequencing were downloaded from the TCGA official website (https://portal.gdc.cancer.gov/) using the TCGAbiolinks R package [28]. A log2 transformation was performed on all data to standardise the format. Survival data from the GSE53624 (Table S2) and TCGA-ESCC (Table S3) datasets were analysed using univariate and multifactorial COX regression analyses.

2.2. Patients

Tissues from 106 patients with ESCC were obtained from the Department of Oesophageal Surgery of the Provincial Hospital of Shandong First Medical University between May and August 2023 (Table S4). The inclusion criteria were as follows: age between 40 and 69 years, no sex restriction, confirmed ESCC as the pathological tissue type, no prior chemotherapy or radiotherapy before surgery, and negative pathological margins. The Union for International Cancer Control and the American Joint Committee on Cancer eighth edition tumour, node, and metastasis classification criteria for ESCC were used to classify all patients with ESCC. This study was approved by the Ethics Committee of the Provincial Hospital of Shandong First Medical University (approval no. NSFC: 2024-619). The experimental methodology and informed consent processes adhered to the guidelines outlined in the Declaration of Helsinki.

2.3. Cell lines

Five ESCC cell lines (HEEC, KYSE410, KYSE30, KYSE150, and KYSE510) were obtained from the Shanghai Institute for Biological Sciences, Chinese Academy of Sciences (Catalogue No. TCHu236). The cell lines were cultivated at 37 °C in Roswell Park Memorial Institute (RPMI)-1640 medium (Kibbutz Beit HaEmek BI) supplemented with 10 % foetal bovine serum (FBS). A total of 15 passages were used in this study. THP-1 monocytes (American Type Culture Collection, VA, USA) were cultured in Dulbecco's modified Eagle's medium containing 10 % FBS. THP-1 cells were treated with 100 ng/mL Phorbol 12-myristate 13-acetate (PMA) (AdipoGen, San Diego, CA, USA) for 24 h to induce differentiation into macrophages. After 24 h of culture, the cells fully adhered to the surface. The cells were stimulated with IL-4 (20 ng/mL) and IL-13 (20 ng/mL) for 24 h to induce M2 polarisation. The THP-1 macrophages were divided into two groups (control and sh-CTSL) for each treatment. After 48 h of culture, the culture medium was replaced with fresh medium, and the cells were further cultured for 24 h. The supernatant was collected and used as the macrophage culture medium for culturing KYSE30 and KYSE150 cells.

2.4. Animal experiments

Six four-week-old female nude mice (Spivey Biotechnology Co., Beijing, China) were randomly assigned into two groups of three each. Following grouping, we injected 100 μL of 1×10^6 cell solution into the right armpit of the mice. The tumour volume was subsequently measured every 5 days using the following formula:

$$V = (L \times W2)/2, \tag{1}$$

where L and W represent the longest and shortest diameter of the tumour.

The Experimental Animal Ethics Committee of the Provincial Hospital of Shandong First Medical University reviewed and approved the use of mice in these experiments (approval number: No. NSFC: 2024-619).

2.5. Enrichment analysis

Using data from TCGA-ESCC and GSE53624 datasets, we uploaded genes exhibiting a correlation greater than 0.5 with *CTSL* to the DAVID database (https://david.ncifcrf.gov/) for annotation and analyses (Table S5). This yielded GO and KEGG enrichment results. The top eight results were sorted according to p-values from highest to lowest ($p < 0.001$). GSVA was used to assess the gene set enrichment results [29]. Utilising immune-related genomic data (Table S6) from the AmiGO 2 database (https://amigo.geneontology.org/amigo), we generated heat maps of the enrichment results using the heatmap software. To investigate the relationship between *CTSL* and immunological processes, Pearson's correlation analysis was performed.

2.6. Immunological analysis

The ESTIMATE R package [30] was used to calculate the immune and stromal scores of all patients. The dataset GSE53624 was used for the validation. To analyse the link between *CTSL* and immune cells, we performed an immune cell infiltration analysis using CIBERSORTx [31], which was further validated using single-sample gene set enrichment analysis [32]. Considering the important role of immunotherapy in tumours, several joint immune checkpoints were also analysed. The TISIDB database (http://cis.hku.hk/TISIDB/) was used to assess immunological significance of *CTSL* in cancer.

2.7. Single-cell data analysis using Seurat

The GSE196756 single-cell sequencing data were imported using the Seurat R package [33] to filter low-quality cells. Subsequently, the cells were grouped into 15 clusters using the FindClusters function with the resolution parameter set to 0.5. Cell type annotation was performed using the SingleR R package [34], and typical marker gene expression was referenced for further clustering annotation (monocytes: *CST3, CD68*, and *CD16*; macrophages: *MSR1* and *CD163*; T cells: *CD2, CD3E*, and *CD3E*; B cells: *CD79A* and *CD37*; endothelial cells: *PECAM1* and *FLI1*; and epithelial cells: *KRT17* and *CSNK2A1*). The single-cell dataset GSE188900 was validated using the same methodology, and further analysis was conducted using the TISCH2 database (http://tisch.comp-genomics.org/).

2.8. Mutation analysis

Based on the somatic data from TCGA-ESCC, we used the maftools R package [35] for statistical analyses, generating waterfall plots using the oncoplot function. Tumour mutational burden (TMB) [36], which refers to the number of mutations in specific genes within a tumour tissue, was calculated using the tmb function in maftools. We used Kaplan–Meier survival curves to demonstrate the difference in patient survival between the high- and low-TMB groups and calculated their correlation with *CTSL*.

2.9. Drug sensitivity analyses

The R package oncPredict [37] was used to obtain the half-maximal inhibitory concentration (IC50) values of the drugs in the GDSC

database. The correlation between drug IC50 values and high and low *CTSL* expression was analysed using Spearman's correlation analysis. Bar graphs were plotted to compare IC50 differences between patients with high and low expression levels.

2.10. Predictive modeling

Based on TCGA-ESCC data, clinical factors such as age, sex, stage, T stage, and N stage were correlated and analysed using one-way COX regression analysis. Factors that significantly correlated with survival were screened ($p < 0.05$) to construct column line graphs. Subsequently, patient survival probabilities at one, two, and three years were calculated. Receiver operating characteristic curves, correction curves, and model discriminatory performance were used to assess the accuracy of the model. The external dataset GSE53624 was used for validation.

2.11. Validation of Mendelian randomization analysis

The GWAS database (https://gwas.mrcieu.ac.uk/) was used to obtain *CTSL* and EC data (Table S7) for two-sample Mendelian randomization with heterogeneity, sensitivity, and pleiotropy analyses. To ensure that genetic variation was not associated with potential confounders (smoking, heavy alcohol consumption, hot beverages, or pickled foods), queries were performed using the Phenoscanner database (http://www.phenoscanner.medschl.cam.ac.uk/). Subsequently, the results were subjected to meta-analysis to verify the robustness of this relationship.

2.12. Western blotting

A small amount of tissue sample was rinsed three times with saline, and radioimmunoprecipitation assay (RIPA) lysis buffer containing phenylmethylsulfonyl fluoride (PMSF) was used to lyse the tissue and cells to extract proteins (RIPA:PMSF:protein phosphatase inhibitor = 100:1:1). Protein samples were separated using 10 % sodium dodecyl sulfate-polyacrylamide gel electrophoresis and transferred to a polyvinylidene difluoride membrane. The calculated primary antibody was added (primary antibody stock was stored at −20 °C), and the closed polyvinylidene difluoride membrane was placed in a centrifuge tube at 4 °C overnight. Next, the membrane was incubated with the corresponding secondary antibody for 1–2 h at 37 °C and placed on a visualiser to develop and save the results, noting positive and negative distinctions. β-Actin was used as an internal reference.

2.13. Real-time quantitative reverse transcription polymerase chain reaction

Following RNA extraction using the RNAiso Plus system (TaKaRa), the total cellular RNA was reverse-transcribed into complementary DNA using an RT kit (TaKaRa). β-Actin was used as an internal reference gene. The primer details are provided in Table S8.

2.14. Lentiviral transfection

Negative control and *CTSL* RNA interference lentiviral vectors were acquired from GeneChem (Shanghai, China). Subsequently, the cells were screened using a medium containing 5 μg/mL puromycin to obtain stable transfected cell lines. The two lentiviral vectors were injected into KYSE150 and KYSE30 cells, respectively.

2.15. Wound-healing assay

After transfection, the cells were seeded into six-well plates during the logarithmic growth phase until they reached 90–95 % confluence. A 200 μL pipette was used to create a vertical scratch in the middle of each well. Scratched cells were incubated in RPMI-1640 medium without FBS for a full day. After 0 and 24 h, the scratches were examined under a microscope, and the wound area was assessed at the same spots using the ImageJ software (V1.8.0). Cell migration rate was calculated as follows:

$$\text{Cell migration area} \times 100\% \,/\, (\text{first scratch area} - \text{scratch area after 24 h}). \quad (2)$$

2.16. Colony formation assay

After cultivation for 10 days, the transfected cells were seeded into six-well plates at 1000 cells/well. Following clonal group formation, cells were fixed using 4 % tissue cell fixative for 20 min at 37 °C. Each well was filled with 1 mL of 0.1 % crystalline violet (McLean, China) and allowed to sit for 2 min. The wells were then washed with PBS to ensure complete removal of the staining solution. This resulted in cell clusters that exhibited a purple hue.

2.17. Transwell assays

The upper and lower compartments of the 24-well Transwell chamber were divided by an 8 μm-pore-sized polycarbonate

membrane. To assess cell invasion, a polycarbonate membrane coated with a gel matrix (Corning) was used as the compartment, and an untreated polycarbonate membrane was used for migration studies. The upper compartment of the Transwell was filled with exponentially treated cell solution, whereas the lower compartment was filled with medium containing 20 % FBS. Cells were allowed to pass through a polycarbonate membrane and enter the lower compartment after 20 h of incubation at 37 °C and 5 % CO_2. The cells were stained with crystal violet and fixed in 4 % paraformaldehyde. Finally, the number of labelled cells that penetrated the polycarbonate membrane and entered the lower compartment was quantified using an inverted microscope.

2.18. EdU cell proliferation assay

In the exponential growth phase, 5000 transfected cells were seeded into 96-well plates and allowed to grow for 36 h. Subsequently, EdU labelling, cell fixation, Apollo staining, and DNA staining were conducted. Images were acquired using an inverted fluorescence microscope.

2.19. Statistical analyses

All statistical analyses were performed using the R software (version 4.1.1). The Wilcoxon rank-sum test was used to compare differences between two groups, whereas the Kruskal–Wallis test was used to assess differences between more than two groups. Correlations were determined using Spearman's correlation analysis. GraphPad Prism 8 was used for statistical analysis of the cellular

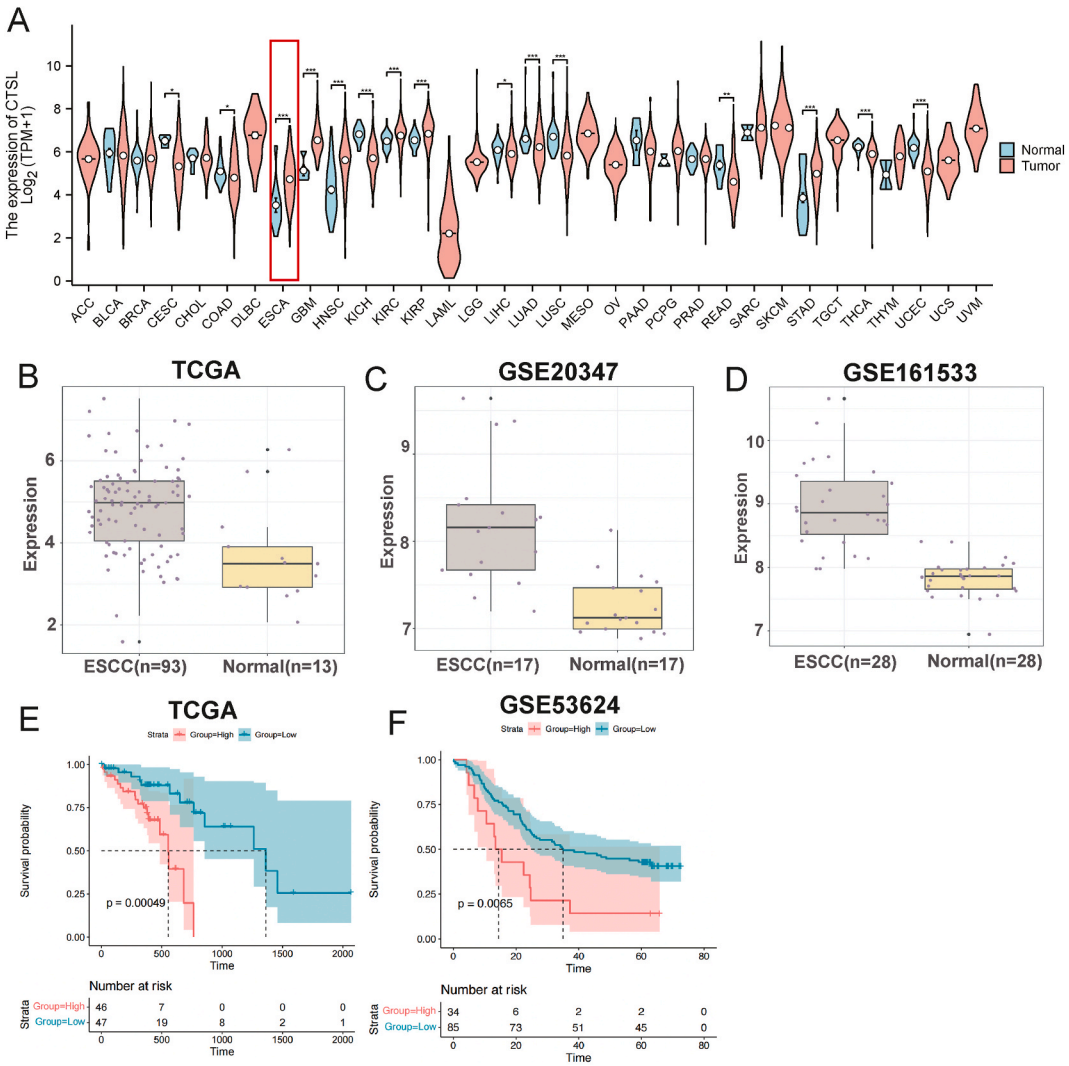

Fig. 1. Expression levels of CTSL in ESCC. **A:** TCGA database of CTSL expression in different cancer datasets. **B–D:** Expression levels of CTSL in tumour tissues and normal tissues. **E:** Kaplan–Meier curves of high and low expression of CTSL in TCGA-ESCC data. **F:** Kaplan–Meier curves of high and low expression of CTSL in GSE53624. *p < 0.05, **p < 0.01, ***p < 0.001. ESCC, oesphageal squamous cell carcinoma.

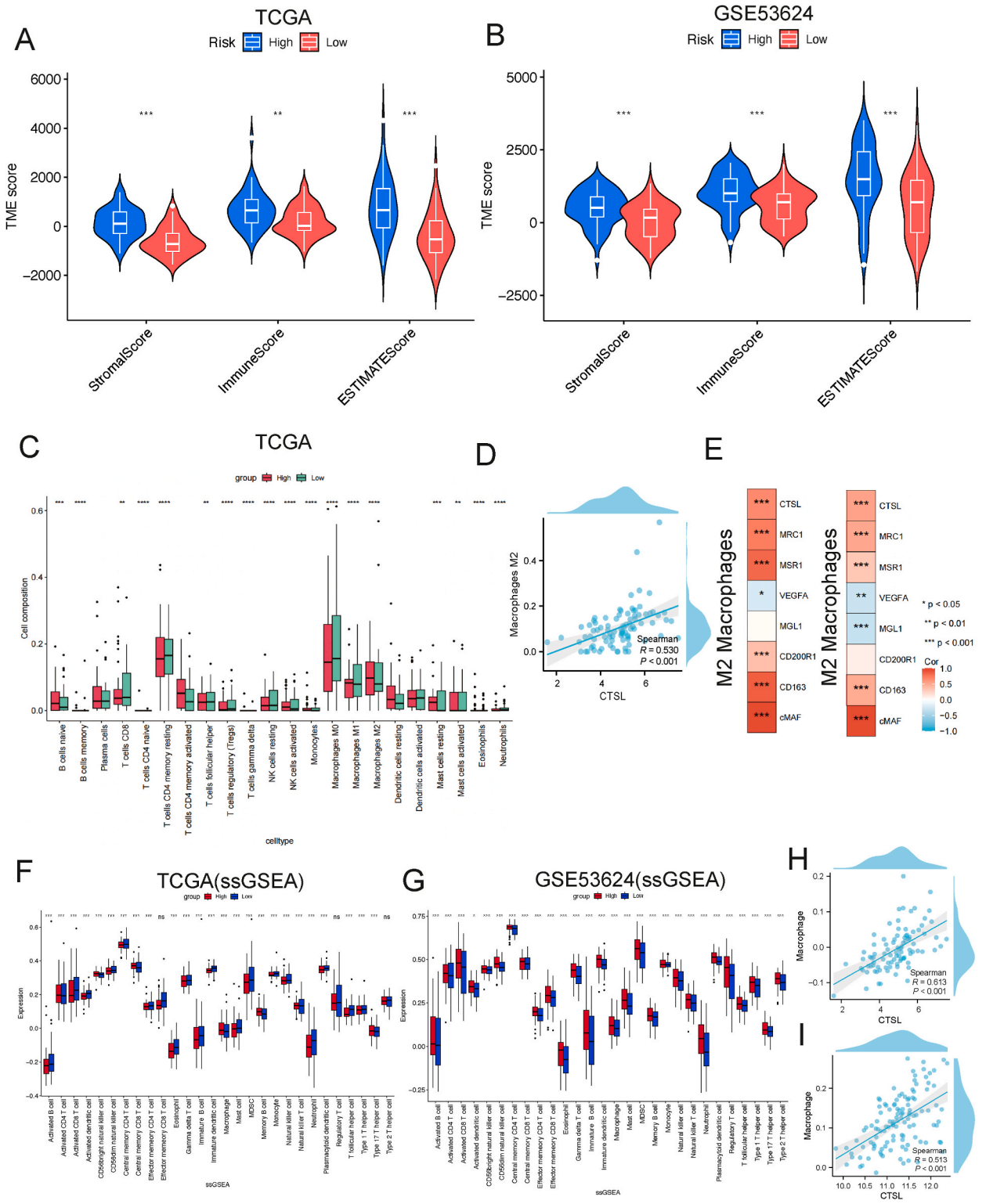

Fig. 2. Immunoassay results. **A, B:** Correlation between CTSL expression and stromal score, immune score, and ESTIMATEScore in TCGA and dataset GSE53624. B: Infiltration of different immune cells in the CIBERSORT analysis. **C:** Correlation between CTSL and M2 macrophages. **D:** Correlation between CTSL and M2 macrophage signature genes in TCGA and dataset GSE53624. **E:** the correlation between CTSL and M2 macrophage signature genes. **F–I:** Infiltration of different immune cells in TCGA and dataset GSE53624, ssGSEA analysis, and correlation between CTSL and macrophages. *p $<$ 0.05, **p $<$ 0.01, ***p $<$ 0.001.

studies, and Student's t-test was used to examine significant differences between the two groups. P-values < 0.05 were considered significant.

3. Results

3.1. CTSL was highly expressed in ESCC

Analyzing the expression data of *CTSL* across various malignant and normal tissues from TCGA, we observed that *CTSL* expression was significantly higher in ESCC tumour tissues ($p < 0.01$; Fig. 1A). This observation was confirmed using the GEPIA database (Fig. S1A and B). Next, we used TCGA database to extract data on *CTSL* expression levels in patients with ESCC and compared them to those in adjacent tissues. *CTSL* expression levels in ESCC tissues were significantly higher than those in paracancerous tissues ($p < 0.001$; Fig. 1B). This trend was confirmed through validation using the GSE20347 (Fig. 1C) and GSE161533 (Fig. 1D) datasets. These findings indicate a considerable increase in *CTSL* expression in tumour tissues compared to that in normal tissues.

3.2. Survival analysis

Kaplan–Meier curves were plotted for patients with ESCC based on median *CTSL* expression. These curves revealed significantly poorer overall survival in the high-risk group than in the low-risk group ($p < 0.01$; Fig. 1E). This pattern was corroborated using the external dataset GSE53624 ($p < 0.01$; Fig. 1F). To further explore the effect of *CTSL* expression on patient survival, internal validation was conducted by grouping TCGA patients into 5:5 and 3:7 ratios, and the results were significantly different ($p < 0.01$; Fig. S1C–F).

3.3. Functional enrichment analyses (GO/KEGG/GSVA)

Based on the TCGA-ESCC dataset, we performed Pearson's correlation analysis for *CTSL*. Correlations exceeding 0.5 were selected for subsequent analysis, and heat maps displaying the top 15 positively and negatively correlated genes were generated (Fig. S2A). Similarly, we performed Pearson's correlation analysis based on the GSE53624 dataset and plotted a heatmap (Fig. S2B). To explore the biological functions associated with *CTSL*, we performed GO and KEGG analyses using TCGA database and the external dataset GSE53624. In TCGA database, the biological processes most relevant to *CTSL* included immune response, inflammatory response, and positive regulation of T cell proliferation (Fig. S2C), whereas the most relevant signalling pathways included complement and coagulation cascades, *Staphylococcus aureus* infection, and osteoclast differentiation (Fig. S2E; Table S9). The biological processes, cellular components, molecular activities, and signalling pathways associated with CTSL in the external dataset GSE53624 were comparable to those in TCGA database (Fig. S2D and F; Table S10). These findings suggested that *CTSL* is crucial for immunological modulation. To confirm this, we conducted GSVA to ascertain the enrichment scores for immunological processes in TCGA (Fig. S3A), and GSE53624 (Fig. S3B) datasets. *CTSL* expression is strongly correlated with every immunological function, indicating its importance in the ESCC immune milieu.

3.4. Relationship between CTSL and immunity

We performed ESTIMATE analysis based on the expression levels of *CTSL* using TCGA-ESCC database (Fig. 2A). The results indicated that higher *CTSL* expression corresponded with elevated ESTIMATEScore ($p < 0.001$) and ImmuneScore ($p < 0.001$). Comparable results were observed when the external dataset, GSE53624, was analysed (Fig. 2B). We established a significant correlation between *CTSL* expression and the infiltration of mast cells, natural killer cells, M0 macrophages, M2 macrophages, and $CD4^+$ T cells, among other immune cells ($p < 0.05$; Fig. 2C). Notably, a robust positive correlation was observed between M2 macrophages ($R = 0.53$, $p < 0.001$; Fig. 2D). Further investigation of the correlation between *CTSL* and M2 macrophage signature genes in TCGA-ESCC and GSE53624 datasets revealed a positive association with most signature genes, reinforcing the notion that *CTSL* most likely affects ESCC progression through TAMs (Fig. 2E). Subsequent single-sample gene set enrichment analysis confirmed these findings (Fig. 2F–I), which were further validated (Fig. S4) from the TISIDB database (http://cis.hku.hk/TISIDB/).

Immune checkpoint inhibitors (ICIs) are widely used in tumour immunotherapy. Based on TCGA-ESCC data, *CTSL* expression positively correlated with multiple immune checkpoints (Fig. S5A and B). This association was further demonstrated using the external dataset GSE53624 (Fig. S5C and D). TCGA database (Fig. S5E and F) and the GSE53624 dataset (Fig. S5G and H) were used to further investigate these associations, owing to the promising efficacy of PD-1 and PD-L1 in a subgroup of patients with ESCC. These findings underscore the potential significance of *CTSL* in tumour immunity.

3.5. Single-cell data analysis

The single-cell dataset GSE196756 was analysed using the harmony method to remove batch effects. Subsequently, we identified 15 sub-clusters at a resolution of 1.0 (Fig. 3A). The cell types within each cluster were identified using the SingleR package (Fig. 3B) and cross-referenced with literature annotations (Fig. 3D). Six cell types were identified: T cells (clusters 0, 1, and 8), B cells (clusters 3 and 9), epithelial cells (clusters 2, 10, and 14), monocytes (clusters 4, 6, 11, and 13), macrophages (clusters 5 and 7), and endothelial cells (cluster 12) (Fig. 3C). Violin plots illustrating cell-type marker and *CTSL* gene localisation further supported the specific expression of *CTSL* in macrophages (Fig. 3E). Subsequently, we used the single-cell dataset GSE188900 for further validation

(Fig. 3F–J). Although distinguishing between macrophages and monocytes based on typical marker gene expression is challenging, we confirmed significant differences in *CTSL* expression in macrophages and monocytes compared with other cell types. This reinforces our previous findings and underscores the close relationship between *CTSL* and immunity. Furthermore, using the TISCH2 database

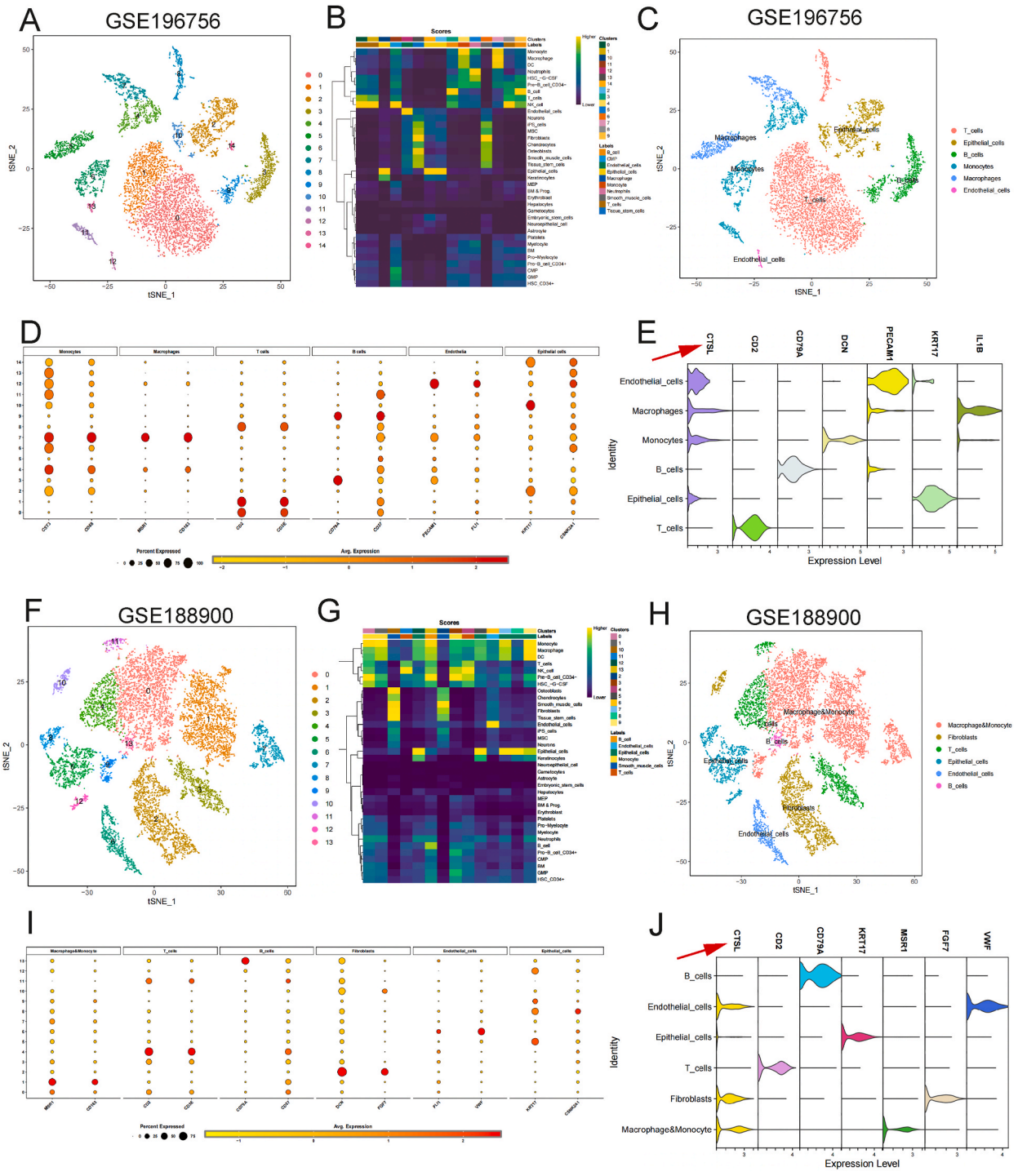

Fig. 3. Single cell analysis. **A:** Reduced dimensional clustering analysis with t-SNE (t-Distributed Stochastic Neighbor Embedding) distribution of different cell clusters with different colors used to label Cluster. **B:** Heatmap of the SingleR package identifying the cell types of each cluster. **C:** Distribution of t-SNE of different cell types. **D:** Differential genes of each cell cluster demonstrated by heatmap. **E:** Labelled genes of each cell type demonstrated by violin map. **F–J:** Single cell dataset GSE188900 for further validation. (For interpretation of the references to color in this figure legend, the reader is referred to the Web version of this article.)

(http://tisch.comp-genomics.org/), we found that *CTSL* was highly expressed in macrophages (Fig. S6A–D).

3.6. Mutation analysis and drug sensitivity prediction

Genome sequencing provided the detailed sequences of the mutated genes. We identified the top 20 high-frequency mutated genes based on the median *CTSL* expression, stratifying patients in the TCGA-ESCC dataset into high- and low-expression populations (Fig. 4A and B). *TP53* and *TTN* were the most frequently mutated genes in both groups. TMB was significantly lower in the high-*CTSL*-expression group than in the low CTSL expression group, and *CTSL* negatively correlated with TMB (Fig. 4C and D). Additionally, we extrapolated the IC50 values of 198 drugs from TCGA-ESCC dataset. Notably, the low-expression group tended to exhibit higher sensitivity to Telomerase. Inhibitor.IX, GSK1904529A, OSI.027, pyridostatin, RO.3306, and P22077, whereas the high-expression group was more sensitive to SB216763 (Fig. 4E–L). These findings offer valuable insights into the clinical treatment strategies and

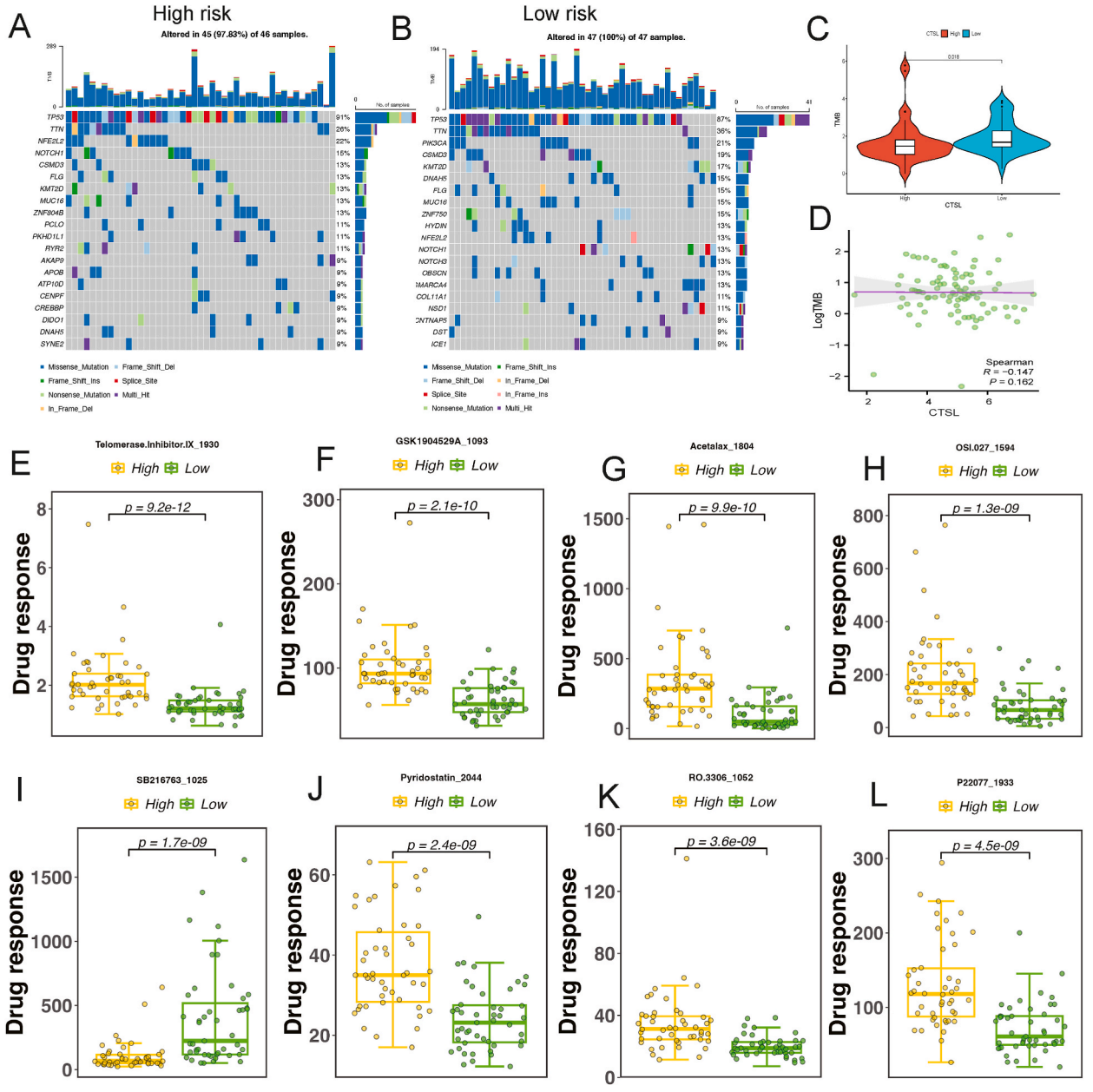

Fig. 4. Mutation analysis and drug sensitivity prediction. **A, B:** Top 20 genes with mutation frequency in high and low expression groups. **C:** Violin plot of CTSL vs. TMB. **D:** Analysis of CTSL vs. TMB. **E–L:** Drug sensitivity analysis. *p < 0.05, **p < 0.01, ***p < 0.001. TMB, tumour mutation burden.

specific information is provided in Table 1.

3.7. Prognostic model construction and validation

Univariate and multivariate COX regression analyses (Fig. 5A and B) were conducted using TCGA-ESCC data to evaluate the diagnostic value of *CTSL* expression, age, sex, and ESCC tumour stage. The results revealed that *CTSL* expression independently correlated with patient prognosis in both univariate and multivariate COX regression analyses ($p < 0.05$). However, no significant correlation was observed between *CTSL* expression and patient prognosis using the dataset GSE53624. Subsequently, we generated a prognostic column-line graph based on the results of the one-way COX analysis (Fig. 5C). For the one-, two- and three-year follow-ups, the areas under the time-dependent receiver operating characteristic curves were 0.719, 0.829, and 0.758, respectively (Fig. 5D). Furthermore, the calibration curves demonstrated a satisfactory fit (Fig. 5E). Validation using the external dataset GSE53624 yielded similar results (Fig. 5F and G), underscoring the potential of *CTSL* expression in assessing patient prognosis.

3.8. Validation of Mendelian randomization analysis

Single nucleotide polymorphisms (SNPs) closely associated with *CTSL* expression data (GWAS ID: ebi-a-GCST90012073) were screened ($p < 1.0 \times 10^{-5}$), and the linkage disequilibrium parameter was set ($R2 < 0.001$, kb = 10,000). We then extracted data from two groups of EC (GWAS ID: ebi-a-GCST90018621 and bbj-a-117) using GWAS and merged the *CTSL* expression data with the final EC datasets individually. SNPs with palindromic sequences were excluded from analysis. Finally, using the inverse variance-weighted method, we identified a potential association between *CTSL* expression and EC (Fig. 6A). This analysis revealed a positive correlation between ebi-a-GCST90012073 and ebi-a-GCST90018621 (odds ratio [OR]:1.22; 95 % confidence interval [CI]: 0.97–1.52; $p = 0.08$). Additionally, ebi-a-GCST90012073 showed a slightly positive correlation with bbj-a-117 in the validation group (OR: 1.21; 95 % CI: 0.96–1.53; $p = 0.1$). No potential horizontal pleiotropy was detected and Cochran's Q results showed no significant heterogeneity among the included SNPs. To explore the results of the analyses, we conducted a comprehensive visual analysis of the two-sample Mendelian randomization results, encompassing scatterplots (Fig. 6B), forest plots (Fig. 6C), leave-one-out sensitivity analysis results (Fig. 6D), and funnel plots (Fig. 6E), along with further validation in the validation group (Fig. 6F–I). Finally, we performed a meta-analysis of the two positive correlations, which showed good results (OR: 1.22; 95 % CI: 1.03–1.43; $p < 0.05$), further supporting our hypothesis (Fig. 6J).

3.9. CTSL promotes ESCC cell proliferation

Protein blotting analyses of ESCC tissue specimens demonstrated significantly higher expression of *CTSL* in ESCC tissues than in adjacent tissues (Fig. 7A and B). Next, we examined the mRNA expression levels of *CTSL* in HEEC and KYSE410, KYSE30, KYSE150, and KYSE510 cells using real-time quantitative reverse transcription polymerase chain reaction. Compared to that in HEEC, the mRNA expression level of *CTSL* was significantly increased in the KYSE410, KYSE30, KYSE150, and KYSE510 cell lines, with the highest expression observed in KYSE30 and KYSE150 cells (Fig. 7C and D). Therefore, these two cell lines were selected for subsequent

Table 1
Detailed information on the top seven sensitive drugs.

Drug name	Drug target	Target pathway	Introduction
Telomerase Inhibitor IX	Telomerase	Genome integrity	Telomerase Inhibitor IX works by inhibiting telomerase activity, thereby limiting the lengthening of chromosome ends. This drug is particularly indicated for rapidly proliferating cancer cells, which typically have high telomerase activity.
GSK1904529A	IGF1R, IR	IGF1R signalling	GSK1904529A works by binding to the HER3 receptor and inhibiting its tyrosine kinase activity. This blocks the interaction between HER3 and other signalling pathway molecules, thereby interfering with relevant signalling in cancer cells.
OSI-027	MTORC1, MTORC2	PI3K/MTOR signalling	OSI-027 works by inhibiting the growth and proliferation of cancer cells through inhibition of the mTOR signalling pathway. mTOR signalling pathway is overactive in many types of cancers, leading to abnormal cell proliferation and survival. By inhibiting the mTOR signalling pathway, OSI-027 is able to block the abnormal proliferation of cancer cells, thereby inhibiting tumour development.
SB216763	GSK3A, GSK3B	WNT signalling	The main action of SB216763 is to intervene in cell signalling by inhibiting GSK-3 activity. It does this by binding to GSK-3 and blocking its phosphorylation of its substrates.
Pyridostatin	G-quadruplex stabiliser	DNA replication	Pyridostatin is a small molecule compound with anticancer activity, and its mechanism of action is mainly related to DNA target binding and stabilisation of the DNA G-quadruplex structure.
RO 3306	CDK1	Cell cycle	The main effect of RO-3306 is to inhibit the activity of CDK1.CDK1 binds to its regulatory subunit cyclin B to form an active complex, which is important for the cell to enter the mitotic phase.RO-3306 blocks the normal progression of the cell cycle by binding to CDK1 and interfering with CDK1's binding to cyclin B.The cell cycle is normally progressed through the cell cycle.
P22077	USP7, USP47	Protein stability and degradation	By binding to HDM2, P22077 is able to block this binding and increase the stability and activity of the p53 protein, and the anti-tumour function of p53 can be reactivated using P22077.

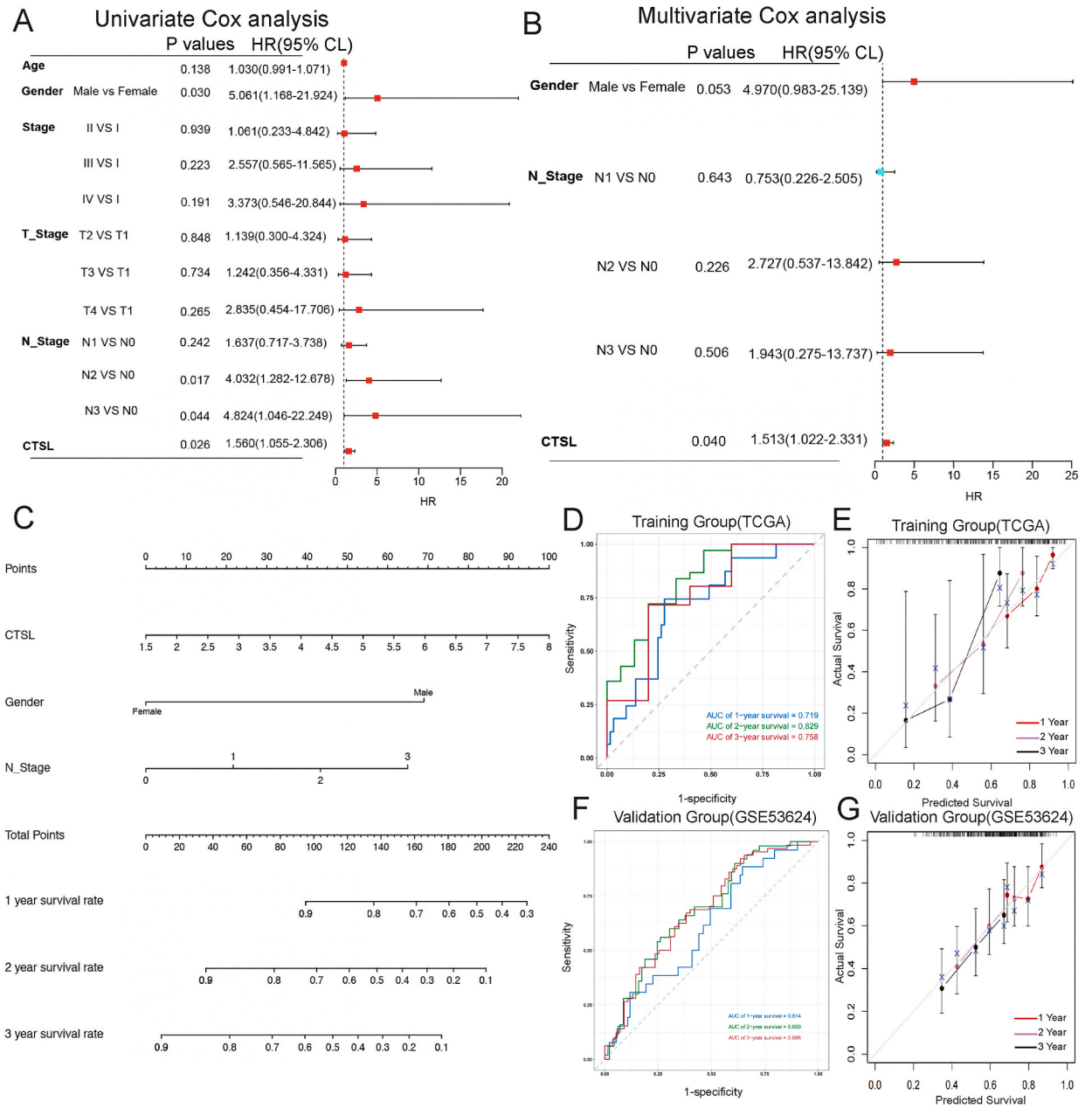

Fig. 5. Construction of CTSL expression-related prediction model. **A, B:** Forest plots of the results of single-factor and multifactor COX regression analyses in the TCGA-ESCC dataset. **C:** Column line plots constructed based on the expression level of CTSL. **D:** ROC curves predicting the feasibility of the predictive model of the nomograms. **E:** Calibration curves of one, two, and three years. **F:** ROC curves of the validation group. **G:** Validation group of one, two, and three years calibration curves.

experiments. First, we transfected lentiviral vectors designed to knock down *CTSL* into KYSE30 and KYSE150 cells and calculated the transfection efficiency (Fig. 7E and F). EdU cell proliferation assays revealed that *CTSL* knockdown significantly reduced the proliferative ability of KYSE30 and KYSE150 cells compared to the control group (Fig. 7G). The wound-healing assay showed that *CTSL* knockdown significantly delayed wound healing (Fig. 7H), and this difference was significant ($p < 0.05$).

3.10. In vitro and in vivo studies of CTSL promotion of ESCC tumour invasion and growth

We also investigated its population-forming ability, which is a crucial characteristic of malignant tumours. Notably, silencing *CTSL* significantly inhibited KYSE30 and KYSE150 cell proliferation in vitro (Fig. 8A). Transwell experiments showed that silencing *CTSL* significantly reduced cell invasion and migration (Fig. 8B). Although our extensive analyses and cellular experiments suggest that *CTSL*

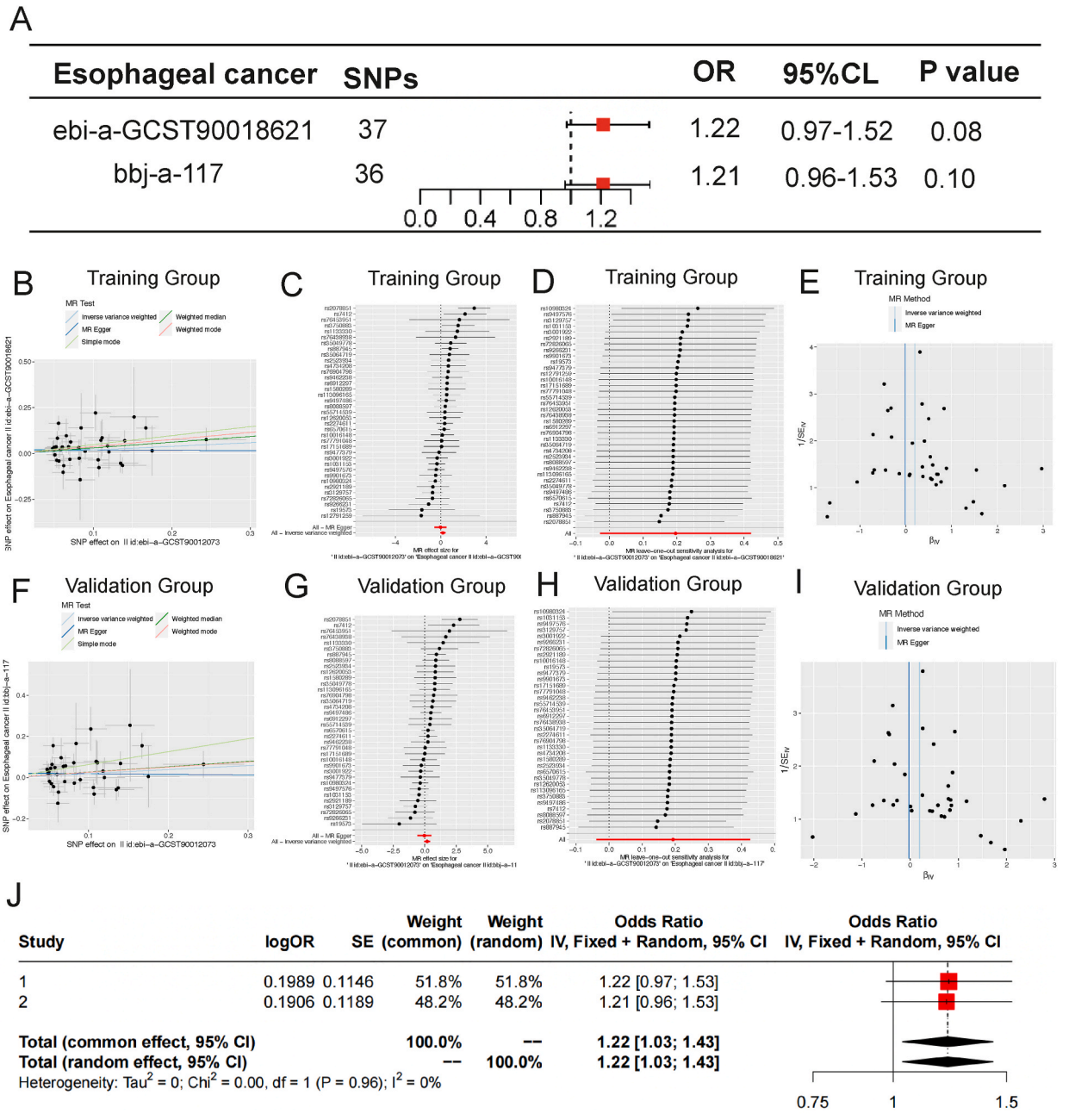

Fig. 6. Mendelian randomization analysis. **A:** Forest plot of Mendelian randomization results for two samples. **B–E:** Scatter plot of Mendelian randomization results for two samples in the experimental group, forest plot, results of leave-one-out sensitivity analysis, and funnel plot. **F–I:** Scatter plot of Mendelian randomization results for two samples in the validation group, forest plot, results of leave-one-out sensitivity analysis, and funnel Figure. **J:** Meta-analysis of a causal relationship between CTSL and EC. EC, oesophageal cancer.

promotes ESCC progression, it is imperative to validate these findings in vivo. Therefore, we subcutaneously inoculated nude mice with KYSE150 cells transfected with *CTSL* knockdown and control (KYSE150) cells. This model demonstrated that *CTSL* knockdown significantly reduced tumour volume and growth rate compared to those in the control group (Fig. 8C). These results suggest that the downregulation of *CTSL* expression reduces the in vivo tumour-forming ability of mice, corroborating the findings of our cellular experiments and bioinformatic analysis.

To further explore the association between CTSL and M2 macrophages, we used bioinformatics to investigate the relationship between CTSL and the M2 macrophage markers (CD163 and CD206). In TCGA database, we found that the expression of CTSL was positively correlated with CD163 ($p < 0.01$, $R = 0.654$) and CD206 ($p < 0.01$, $R = 0.524$; Fig. 9A). We validated these findings using

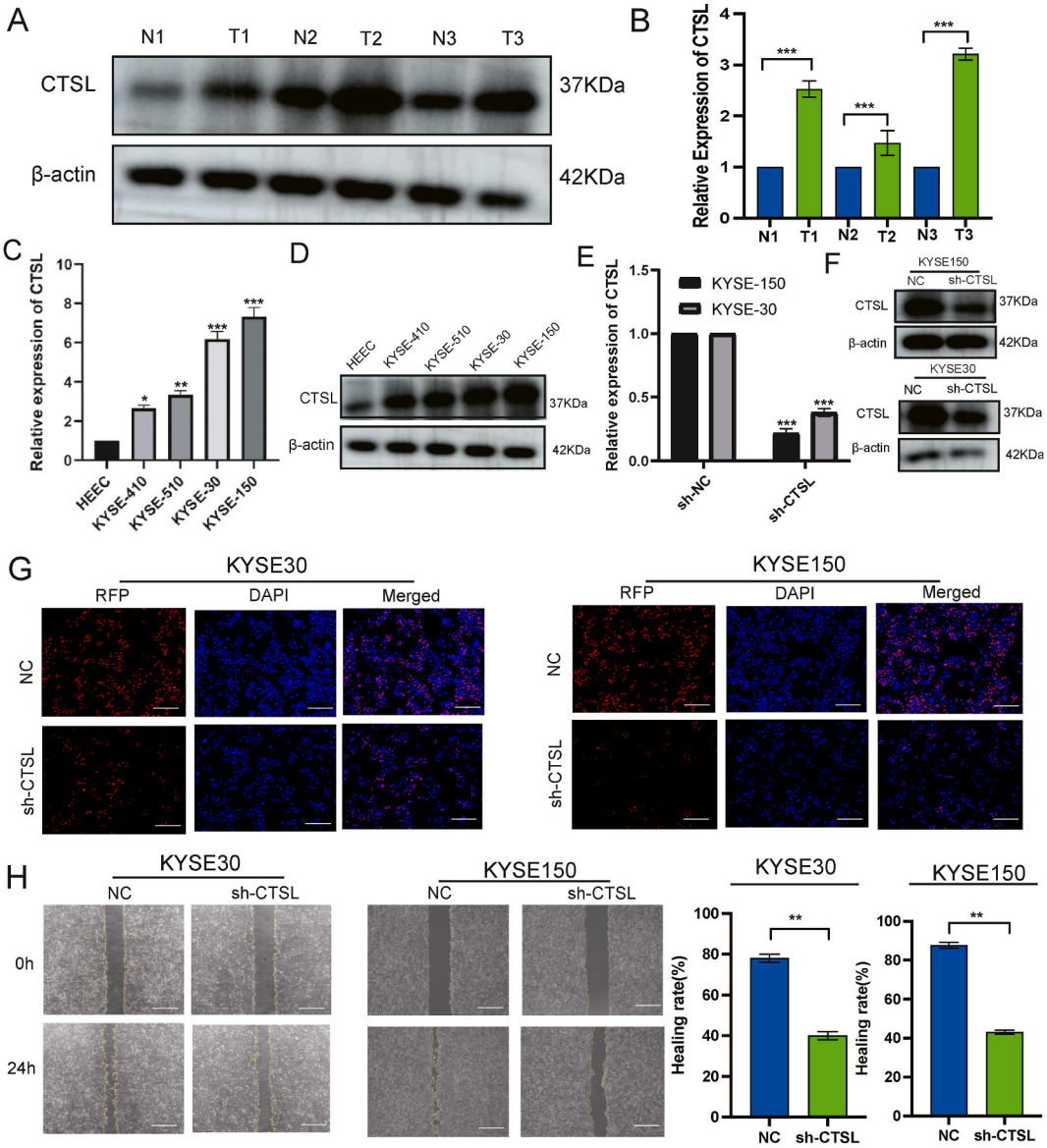

Fig. 7. CTSL promotes the proliferation of ESCC cells. **A:** Protein immunoblotting to detect the expression of CTSL in ESCC and adjacent tissues. **B:** Protein immunoblotting for CTSL expression histograms. **C, D:** qRT-PCR to detect the mRNA expression of CTSL in HEEC, KYSE410, KYSE30, KYSE150, and KYSE510 cell lines for mRNA expression. **E, F:** Transfection efficiency of lentiviral vectors. **G:** EdU cell proliferation assay to detect their proliferation. **H:** Wound healing assay to detect wound healing. *p < 0.05, **p < 0.01, ***p < 0.001. Scale bars: 100 μm. ESCC, oesphageal squamous cell carcinoma.

the external GSE53624 dataset (Fig. 9B). PMA stimulation of THP-1 monocytes to differentiate into macrophages is the most common method for inducing monocyte-macrophage polarisation. We assessed the changes in the expression of the macrophage markers CD14 and CD11b in THP-1 cells after PMA treatment using RT-qPCR. These results indicate the successful differentiation of THP-1 cells into macrophage-like cells (Fig. 9C). Importantly, compared with the control group, macrophages treated with sh-CTSL showed a reduction in M2 polarisation markers CD206 and CD163 after stimulation (Fig. 9D). Subsequently, we co-cultured the supernatant of THP-1 macrophages treated with sh-CTSL or the control with KYSE30 and KYSE150 cells for 24 h (Fig. 9E) and found that the migratory and proliferative abilities of ESCC cells were reduced when cultured with the supernatant from sh-CTSL-treated macrophages (Fig. 9F and G). To further validate our findings, we explored the relationship between CTSL overexpression and polarisation, and found that CTSL overexpression promoted polarisation, leading to ESCC invasion and proliferation (Fig. S7). These results indicate that CTSL promotes macrophage polarisation, and knockdown of CTSL expression inhibits macrophage polarisation in a direction favourable for tumour growth, thereby suppressing the proliferation and migration of ESCC cells.

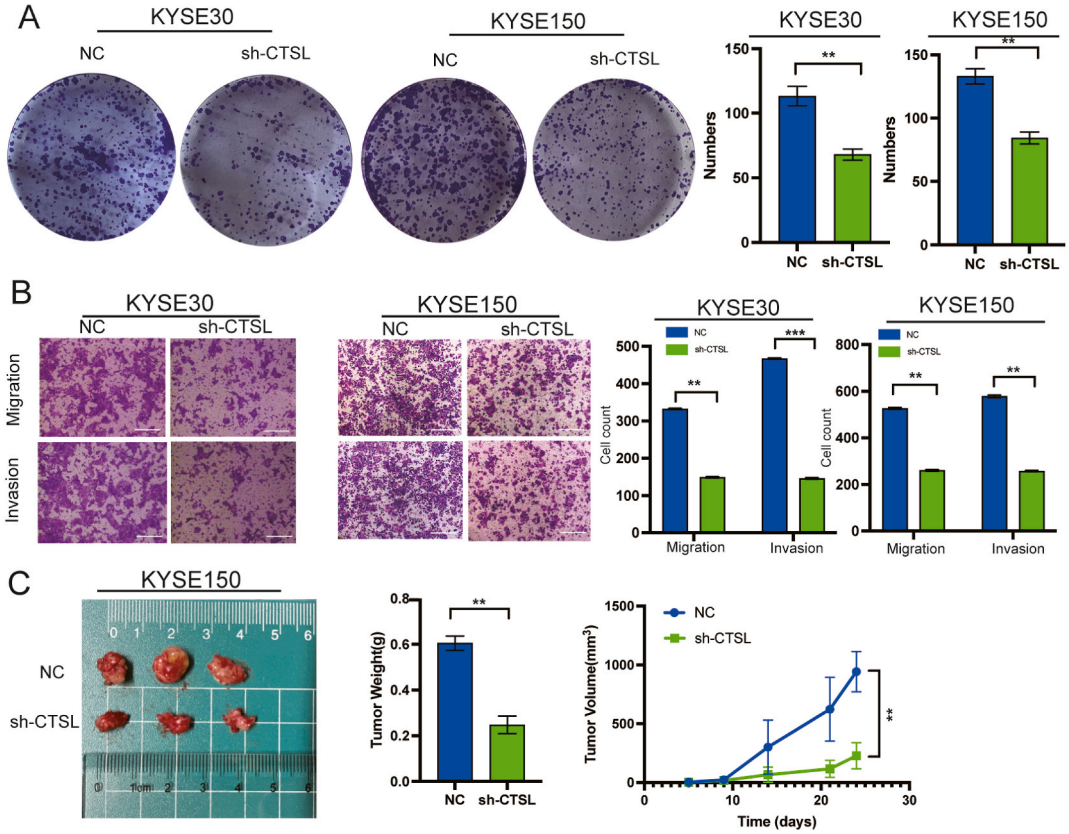

Fig. 8. CTSL promotes ESCC tumour invasion and growth. **A:** Knockdown of CTSL reduces cell proliferation and colony formation. **B:** Cell migration of knockdown CTSL cells was analysed by Transwell analysis. **C:** Knockdown of CTSL inhibits tumour growth in a mouse xenograft model. *p < 0.05, **p < 0.01, ***p < 0.001. Scale bars: 100 μm. ESCC, oesphageal squamous cell carcinoma.

4. Discussion

Recent global cancer statistics indicate that approximately 570,000 newly diagnosed cases of ESCC annually, with China accounting for 50 % [38]. Despite promising advances in medical treatment, the five-year overall survival rate for ESCC remains below 20 % [39], posing a considerable challenge to global health and safety. In this study, we discovered elevated *CTSL* expression in ESCC, which correlated with survival prognosis. In the TME, *CTSL* is closely associated with cellular immunity, particularly TAMs, and immune checkpoints. To our knowledge, this is the first study demonstrating the important role of *CTSL* in ESCC, particularly in its interaction with TAMs. Additionally, our innovative Mendelian randomization analysis revealed the potential of *CTSL* to cause ESCC. In both the in vivo and in vitro assays, *CTSL* promoted ESCC cell proliferation and migration. These results suggested that *CTSL* is a key gene in ESCC.

In this study, we examined *CTSL* expression and its predictive ability in ESCC using various bioinformatic techniques. Elevated *CTSL* expression is associated with lower survival rates in patients with ESCC. Subsequently, we explored the molecular mechanisms and signalling pathways associated with *CTSL* using GO functional enrichment, KEGG pathway, and GSVA approaches. Our results revealed a strong correlation between *CTSL* and immunological responses. Previous studies have linked the immune response to ESCC development [40–42]. Thus, we hypothesised that *CTSL*, through its involvement in the immune response, may control the progression of ESCC. Notably, our single-cell analysis revealed that *CTSL* is highly expressed in monocytes and macrophages, specifically in M2 macrophages. Previous research has also shown that *CTSL* passes through macrophages during lung adenocarcinoma progression [17], aligning with our results and suggesting a potential association between *CTSL* and TAMs.

The TME is closely related to the occurrence and development of tumours [43]. TAMs are the most abundant type of inflammatory cells in the TME, and their role in human tumours has received considerable attention [44]. Numerous studies have confirmed that the presence of TAMs promotes cancer cell proliferation and growth and is closely associated with various behaviours, such as tumour growth, infiltration, and metastasis [45–47]. Furthermore, under specific TME signalling stimulation, TAMs demonstrate considerable plasticity, providing an important entry point for cancer treatments. For example, IL-32 promotes M2 macrophage polarisation and lung metastasis in ESCC through the FAK/STAT3 pathway [48]. Increasing evidence has demonstrated the tumour-promoting role of M2 macrophages in the TME. Therefore, the targeting of M2 macrophages may be a promising strategy for cancer treatment. In this study, we found a significant positive correlation between *CTSL* and M2 macrophage markers, suggesting that *CTSL* influences ESCC

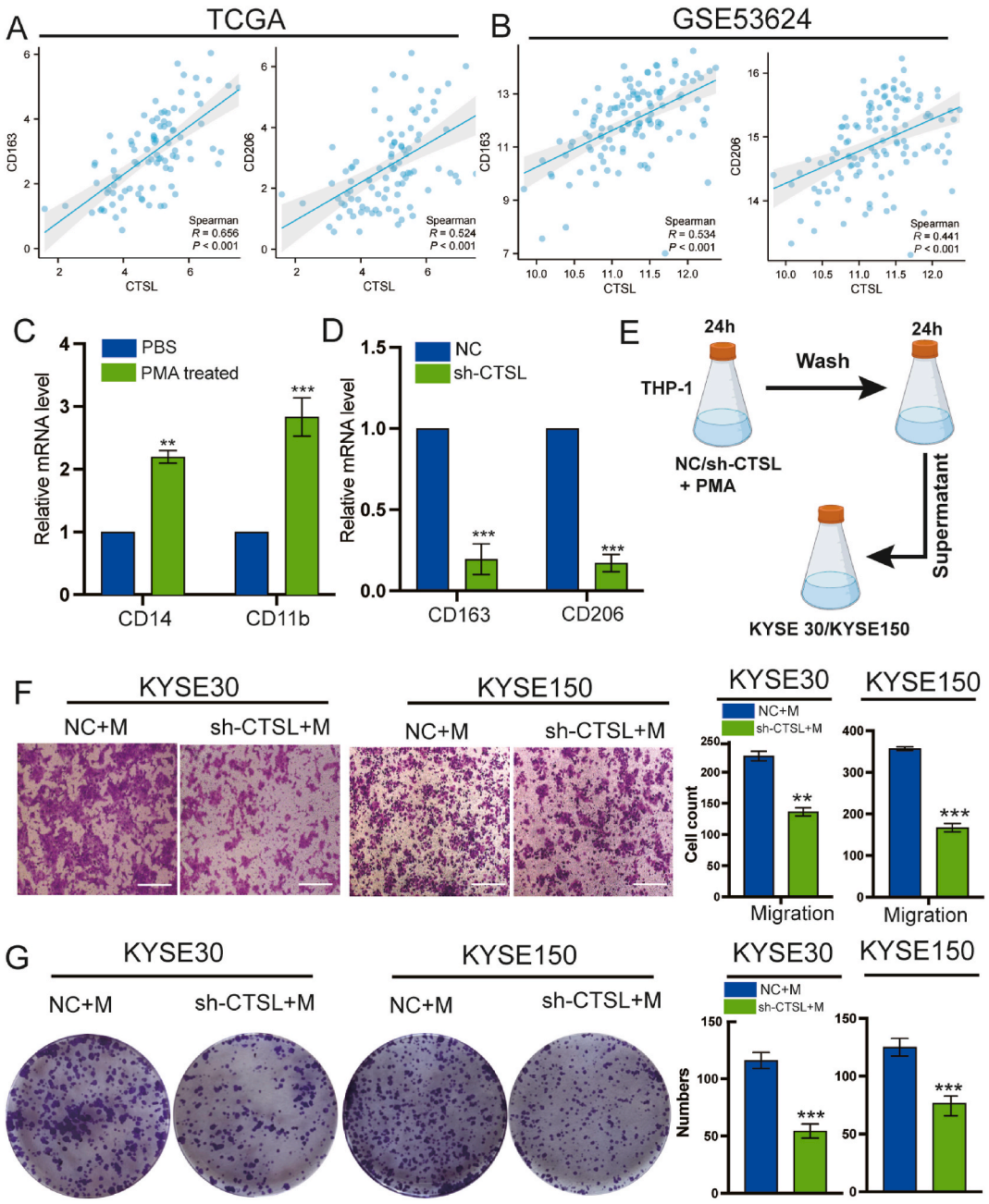

Fig. 9. CTSL promotes the progression of ESCC by regulating macrophage polarisation. **A, B:** Pearson correlation analysis of CTSL expression and M2 macrophage markers (CD 206 and CD 163) in TCGA database and external dataset GSE53624. **C:** RT-qPCR detection of changes in CD 14 and CD 11b mRNA expression in PMA-treated THP-1 cells. **D:** RT-qPCR detection of the expression of M2 polarisation markers CD 206 and CD 163 in sh-CTSL-treated THP-1 macrophages after stimulation. **E:** Co-culture of supernatants from sh-CTSL and control-treated THP-1 macrophages with KYSE30 and KYSE150 cells for 24 h. **F-G:** Reduced migration and proliferation capacities of ESCC cells cultured with supernatant from sh-CTSL-treated macrophages. *p < 0.05, **p < 0.01, ***p < 0.001. Scale bars: 100 μm.

progression by promoting macrophage polarisation. This undoubtedly enhances our understanding of the TAM regulatory mechanisms in tumours and provides new insights into the development of potential therapeutic targets.

The combination of immunity and stromal scores allows for a more precise prediction of patient responsiveness to immunotherapy. Both factors exhibited significant differences in our study, underscoring the efficacy of *CTSL* as an immunotherapy biomarker. We also explored the correlation between *CTSL* expression and the conventional immune checkpoint PD-L1/PD-1 and found that high *CTSL* expression was positively correlated with PD-L1/PD-1 expression, suggesting that immunotherapy targeting PD-L1/PD-1 may be particularly effective in patients with high-*CTSL*-expression group. A recent phase II clinical trial demonstrated significant antitumor

efficacy and a tolerable safety profile of preoperative use of a PD-1 inhibitor (karelizumab) in patients with ESCC [49]. Additionally, $CD8^+$ Tex-SPRY1 cells have been shown to enhance antitumor immune responses and serve as valid predictive biomarkers for PD-1 inhibitor-based NICB therapy [50]. These clinical experiments validated the findings of this study. Detection of *CTSL* expression may aid in the screening of therapeutic drugs for patients with ESCC. By comparing the IC50 values, we evaluated the responsiveness of patients with high and low *CTSL* expression to chemotherapeutic drugs. Our results indicated that patients with low *CTSL* expression were more responsive to GSK1904529A and pyridostatin, whereas patients with high CTSL expression were more responsive to SB216763. These results provide valuable guidance for the treatment of patients with ESCC.

Our analysis of clinical samples from both ESCC and adjacent tissues revealed a high expression of *CTSL* in ESCC. Furthermore, our in vitro and in vivo experiments provide compelling evidence for the oncogenic role of *CTSL* in ESCC progression and metastasis. Colony formation and transwell assays, as well as an established mouse model, showed that *CTSL* knockdown significantly reduced the proliferation and migration abilities of ESCC cells, supporting our bioinformatics analysis. At the same time, we demonstrated a clear positive correlation between *CTSL* and specific markers of M2 macrophages, suggesting that *CTSL* may influence the progression of ESCC by promoting macrophage polarisation. However, further investigation with a larger sample size and additional in vivo evidence is warranted to determine whether the expression of *CTSL* is persistently elevated during tumour progression.

Although we systematically analysed the relationship between *CTSL* expression and ESCC and cross-validated the results using different databases, as well as in vivo and in vitro experiments, this study had some limitations. First, the relatively small sample size, particularly for single-cell RNA sequencing, may limit the generalisability of our findings. Second, although our experiments yielded several interesting findings, there are some limitations to the correlation between *CTSL* and immune macrophages or immune checkpoints. Our research mainly focused on discovering the correlation between high expression of *CTSL* and cellular components in the TME, especially macrophages, but did not deeply explore the mechanism underlying the interaction between *CTSL* function and TAMs. Future studies should focus on using more immune cell lines and animal models to comprehensively understand the role of *CTSL* in immune responses.

In conclusion, our findings suggest that *CTSL* is a critical gene in ESCC that affects patient prognosis and immunity and may be associated with M2 macrophages. Therefore, targeting or modulating CTSL levels may provide new therapeutic strategies for patients with ESCC. Moreover, this study provides a reliable basis for the individualised management and treatment of patients with ESCC.

Funding

This study was supported by the National Science Foundation of Shandong Province, China (Grant No. ZR2019MH092).

Ethics approval and consent to participate

This study was approved by the Ethical Review Committee of Shandong Provincial Hospital affiliated with Shandong First Medical University (approval number: No. NSFC: 2024-619). The requirement for informed consent was waived because the data were de-identified.

Data availability statement

The data supporting the conclusions of this study were included in this article and supplementary materials. The data used and analysed in the current study are available from the corresponding author upon a reasonable request.

CRediT authorship contribution statement

Zhenhu Zhang: Conceptualization. **Jianyu Wang:** Data curation. **Yamin Shi:** Formal analysis. **Ben Wang:** Investigation. **Dong Wang:** Funding acquisition.

Declaration of competing interest

We declare that we have no financial or personal relationships with other people or organizations that could inappropriately influence our work within the submitted manuscript. We also declare that no financial support for the work has influenced its outcome. We further declare that we have no conflicts of interest with respect to the research, authorship, and/or publication of this article.

Appendix A. Supplementary data

Supplementary data to this article can be found online at https://doi.org/10.1016/j.heliyon.2024.e29273.

References

[1] H. Sung, J. Ferlay, R.L. Siegel, M. Laversanne, I. Soerjomataram, A. Jemal, F. Bray, Global cancer statistics 2020: GLOBOCAN estimates of incidence and mortality worldwide for 36 cancers in 185 countries, CA A Cancer J. Clin. 71 (2021) 209–249.

[2] M. Arnold, I. Soerjomataram, J. Ferlay, D. Forman, Global incidence of oesophageal cancer by histological subtype in 2012, Gut 64 (2015) 381–387.

[3] A. Etemadi, H. Poustchi, C.M. Chang, A.M. Calafat, B.C. Blount, D. Bhandari, L. Wang, G. Roshandel, A. Alexandridis, J.C. Botelho, B. Xia, Y. Wang, C.S. Sosnoff, J. Feng, M. Nalini, M. Khoshnia, A. Pourshams, M. Sotoudeh, M.H. Gail, S.M. Dawsey, F. Kamangar, P. Boffetta, P. Brennan, C.C. Abnet, R. Malekzadeh, N. D. Freedman, Exposure to polycyclic aromatic hydrocarbons, volatile organic compounds, and tobacco-specific nitrosamines and incidence of esophageal cancer, J. Natl. Cancer Inst. (2023).

[4] Y. Peng, C. Liu, M. Li, W. Li, M. Zhang, X. Jiang, Y. Chang, L. Liu, F. Wang, Q. Zhao, Identification of a prognostic and therapeutic immune signature associated with hepatocellular carcinoma, Cancer Cell Int. 21 (2021) 98.

[5] P. Huang, X. Zhou, M. Zheng, Y. Yu, G. Jin, S. Zhang, Regulatory T cells are associated with the tumor immune microenvironment and immunotherapy response in triple-negative breast cancer, Front. Immunol. 14 (2023) 1263537.

[6] X. Wu, Z. Zhou, Q. Cao, Y. Chen, J. Gong, Q. Zhang, Y. Qiang, Y. Lu, G. Cao, Reprogramming of Treg cells in the inflammatory microenvironment during immunotherapy: a literature review, Front. Immunol. 14 (2023) 1268188.

[7] L. Yang, Q. Zhao, X. Wang, C. Pilapong, Y. Li, J. Zou, J. Jin, J. Rong, Investigation on the regulatory T cells signature and relevant Foxp3/STAT3 axis in esophageal cancer, Cancer Med. 12 (2023) 4993–5008.

[8] C. Zhang, H. Palashati, Q. Tan, W. Ku, Y. Miao, H. Xiong, Z. Lu, Immediate and substantial evolution of T-cell repertoire in peripheral blood and tumor microenvironment of patients with esophageal squamous cell carcinoma treated with preoperative chemotherapy, Carcinogenesis 39 (2018) 1389–1398.

[9] Y. Mai, J. Su, C. Yang, C. Xia, L. Fu, The strategies to cure cancer patients by eradicating cancer stem-like cells, Mol. Cancer 22 (2023) 171.

[10] B. Liu, B. Zhang, J. Qi, H. Zhou, L. Tan, J. Huang, J. Huang, X. Fang, L. Gong, J. Luo, S. Liu, L. Fu, F. Ling, S. Ma, D. Lai-Wan Kwong, X. Wang, X.Y. Guan, Targeting MFGE8 secreted by cancer-associated fibroblasts blocks angiogenesis and metastasis in esophageal squamous cell carcinoma, Proc. Natl. Acad. Sci. U. S. A. 120 (2023) e2307914120.

[11] Y. Gao, W. Guo, X. Geng, Y. Zhang, G. Zhang, B. Qiu, F. Tan, Q. Xue, S. Gao, J. He, Prognostic value of tumor-infiltrating lymphocytes in esophageal cancer: an updated meta-analysis of 30 studies with 5,122 patients, Ann. Transl. Med. 8 (2020) 822.

[12] J. Hao, M. Li, T. Zhang, H. Yu, Y. Liu, Y. Xue, R. An, S. Wang, Prognostic value of tumor-infiltrating lymphocytes differs depending on lymphocyte subsets in esophageal squamous cell carcinoma: an updated meta-analysis, Front. Oncol. 10 (2020) 614.

[13] E. Cendrowicz, Z. Sas, E. Bremer, T.P. Rygiel, The role of macrophages in cancer development and therapy, Cancers 13 (2021).

[14] A.A. Barkal, R.E. Brewer, M. Markovic, M. Kowarsky, S.A. Barkal, B.W. Zaro, V. Krishnan, J. Hatakeyama, O. Dorigo, L.J. Barkal, I.L. Weissman, CD24 signalling through macrophage Siglec-10 is a target for cancer immunotherapy, Nature 572 (2019) 392–396.

[15] A. Fujishima, Y. Imai, T. Nomura, Y. Fujisawa, Y. Yamamoto, T. Sugawara, The crystal structure of human cathepsin L complexed with E-64, FEBS Lett. 407 (1997) 47–50.

[16] J. Dennemarker, T. Lohmuller, S. Muller, S.V. Aguilar, D.J. Tobin, C. Peters, T. Reinheckel, Impaired turnover of autophagolysosomes in cathepsin L deficiency, Biol. Chem. 391 (2010) 913–922.

[17] L. Huang, N. Lou, T. Xie, L. Tang, X. Han, Y. Shi, Identification of an antigen-presenting cells/T/NK cells-related gene signature to predict prognosis and CTSL to predict immunotherapeutic response for lung adenocarcinoma: an integrated analysis of bulk and single-cell RNA sequencing, Cancer Immunol. Immunother. 72 (2023) 3259–3277.

[18] Q. Chen, J. Fei, L. Wu, Z. Jiang, Y. Wu, Y. Zheng, G. Lu, Detection of cathepsin B, cathepsin L, cystatin C, urokinase plasminogen activator and urokinase plasminogen activator receptor in the sera of lung cancer patients, Oncol. Lett. 2 (2011) 693–699.

[19] H. Kirschke, R. Eerola, V.K. Hopsu-Havu, D. Bromme, E. Vuorio, Antisense RNA inhibition of cathepsin L expression reduces tumorigenicity of malignant cells, Eur. J. Cancer 36 (2000) 787–795.

[20] S. Krueger, U. Kellner, F. Buehling, A. Roessner, Cathepsin L antisense oligonucleotides in a human osteosarcoma cell line: effects on the invasive phenotype, Cancer Gene Ther. 8 (2001) 522–528.

[21] N. Levicar, R.A. Dewey, E. Daley, T.E. Bates, D. Davies, J. Kos, G.J. Pilkington, T.T. Lah, Selective suppression of cathepsin L by antisense cDNA impairs human brain tumor cell invasion in vitro and promotes apoptosis, Cancer Gene Ther. 10 (2003) 141–151.

[22] Z. Yang, J.L. Cox, Cathepsin L increases invasion and migration of B16 melanoma, Cancer Cell Int. 7 (2007) 8.

[23] J. Li, Z. Chen, L. Tian, C. Zhou, M.Y. He, Y. Gao, S. Wang, F. Zhou, S. Shi, X. Feng, N. Sun, Z. Liu, G. Skogerboe, J. Dong, R. Yao, Y. Zhao, J. Sun, B. Zhang, Y. Yu, X. Shi, M. Luo, K. Shao, N. Li, B. Qiu, F. Tan, R. Chen, J. He, LncRNA profile study reveals a three-lncRNA signature associated with the survival of patients with oesophageal squamous cell carcinoma, Gut 63 (2014) 1700–1710.

[24] Z. Shen, M. Chen, F. Luo, H. Xu, P. Zhang, J. Lin, M. Kang, Identification of key genes and pathways associated with paclitaxel resistance in esophageal squamous cell carcinoma based on bioinformatics analysis, Front. Genet. 12 (2021) 671639.

[25] N. Hu, R.J. Clifford, H.H. Yang, C. Wang, A.M. Goldstein, T. Ding, P.R. Taylor, M.P. Lee, Genome wide analysis of DNA copy number neutral loss of heterozygosity (CNNLOH) and its relation to gene expression in esophageal squamous cell carcinoma, BMC Genom. 11 (2010) 576.

[26] K. Shi, Y. Li, L. Yang, Z. Zhang, D. Guo, J. Zhang, Y. Lu, Profiling transcriptional heterogeneity of epithelium, fibroblasts, and immune cells in esophageal squamous cell carcinoma by single-cell RNA sequencing, Faseb. J. 36 (2022) e22620.

[27] X. Pan, J. Wang, L. Guo, F. Na, J. Du, X. Chen, A. Zhong, L. Zhao, L. Zhang, M. Zhang, X. Wan, M. Wang, H. Liu, S. Dai, P. Tan, J. Chen, Y. Liu, B. Hu, C. Chen, Identifying a confused cell identity for esophageal squamous cell carcinoma, Signal Transduct. Targeted Ther. 7 (2022) 122.

[28] A. Colaprico, T.C. Silva, C. Olsen, L. Garofano, C. Cava, D. Garolini, T.S. Sabedot, T.M. Malta, S.M. Pagnotta, I. Castiglioni, M. Ceccarelli, G. Bontempi, H. Noushmehr, TCGAbiolinks: an R/Bioconductor package for integrative analysis of TCGA data, Nucleic Acids Res. 44 (2016) e71.

[29] M.R. Ferreira, G.A. Santos, C.A. Biagi, W.A. Silva Junior, W.F. Zambuzzi, GSVA score reveals molecular signatures from transcriptomes for biomaterials comparison, J. Biomed. Mater. Res. 109 (2021) 1004–1014.

[30] K. Yoshihara, M. Shahmoradgoli, E. Martinez, R. Vegesna, H. Kim, W. Torres-Garcia, V. Trevino, H. Shen, P.W. Laird, D.A. Levine, S.L. Carter, G. Getz, K. Stemke-Hale, G.B. Mills, R.G. Verhaak, Inferring tumour purity and stromal and immune cell admixture from expression data, Nat. Commun. 4 (2013) 2612.

[31] B. Chen, M.S. Khodadoust, C.L. Liu, A.M. Newman, A.A. Alizadeh, Profiling tumor infiltrating immune cells with CIBERSORT, Methods Mol. Biol. 1711 (2018) 243–259.

[32] Y. Chen, Y. Feng, F. Yan, Y. Zhao, H. Zhao, Y. Guo, A novel immune-related gene signature to identify the tumor microenvironment and prognose disease among patients with oral squamous cell carcinoma patients using ssGSEA: a bioinformatics and biological validation study, Front. Immunol. 13 (2022) 922195.

[33] Y. Hao, S. Hao, E. Andersen-Nissen, W.M. Mauck 3rd, S. Zheng, A. Butler, M.J. Lee, A.J. Wilk, C. Darby, M. Zager, P. Hoffman, M. Stoeckius, E. Papalexi, E. P. Mimitou, J. Jain, A. Srivastava, T. Stuart, L.M. Fleming, B. Yeung, A.J. Rogers, J.M. McElrath, C.A. Blish, R. Gottardo, P. Smibert, R. Satija, Integrated analysis of multimodal single-cell data, Cell 184 (2021) 3573–3587, e3529.

[34] D. Aran, A.P. Looney, L. Liu, E. Wu, V. Fong, A. Hsu, S. Chak, R.P. Naikawadi, P.J. Wolters, A.R. Abate, A.J. Butte, M. Bhattacharya, Reference-based analysis of lung single-cell sequencing reveals a transitional profibrotic macrophage, Nat. Immunol. 20 (2019) 163–172.

[35] A. Mayakonda, D.C. Lin, Y. Assenov, C. Plass, H.P. Koeffler, Maftools: efficient and comprehensive analysis of somatic variants in cancer, Genome Res. 28 (2018) 1747–1756.

[36] P. Jiang, S. Gu, D. Pan, J. Fu, A. Sahu, X. Hu, Z. Li, N. Traugh, X. Bu, B. Li, J. Liu, G.J. Freeman, M.A. Brown, K.W. Wucherpfennig, X.S. Liu, Signatures of T cell dysfunction and exclusion predict cancer immunotherapy response, Nat. Med. 24 (2018) 1550–1558.

[37] P. Geeleher, N. Cox, R.S. Huang, pRRophetic: an R package for prediction of clinical chemotherapeutic response from tumor gene expression levels, PLoS One 9 (2014) e107468.

[38] C.S. Yang, X.L. Chen, Research on esophageal cancer: with personal perspectives from studies in China and Kenya, Int. J. Cancer 149 (2021) 264–276.

[39] A. Herskovic, W. Russell, M. Liptay, M.J. Fidler, M. Al-Sarraf, Esophageal carcinoma advances in treatment results for locally advanced disease: review, Ann. Oncol. 23 (2012) 1095–1103.
[40] J. Wen, S. Fang, Y. Hu, M. Xi, Z. Weng, C. Pan, K. Luo, Y. Ling, R. Lai, X. Xie, X. Lin, T. Lin, J. Chen, Q. Liu, J. Fu, H. Yang, Impacts of neoadjuvant chemoradiotherapy on the immune landscape of esophageal squamous cell carcinoma, EBioMedicine 86 (2022) 104371.
[41] J. Yao, Q. Cui, W. Fan, Y. Ma, Y. Chen, T. Liu, X. Zhang, Y. Xi, C. Wang, L. Peng, Y. Luo, A. Lin, W. Guo, L. Lin, Y. Lin, W. Tan, D. Lin, C. Wu, J. Wang, Single-cell transcriptomic analysis in a mouse model deciphers cell transition states in the multistep development of esophageal cancer, Nat. Commun. 11 (2020) 3715.
[42] Z.W. Gao, L. Yang, C. Liu, X. Wang, W.T. Guo, H.Z. Zhang, K. Dong, Distinct roles of adenosine deaminase isoenzymes ADA1 and ADA2: a pan-cancer analysis, Front. Immunol. 13 (2022) 903461.
[43] K. Khalaf, D. Hana, J.T. Chou, C. Singh, A. Mackiewicz, M. Kaczmarek, Aspects of the tumor microenvironment involved in immune resistance and drug resistance, Front. Immunol. 12 (2021) 656364.
[44] A. Lapenna, M. De Palma, C.E. Lewis, Perivascular macrophages in health and disease, Nat. Rev. Immunol. 18 (2018) 689–702.
[45] A.K. Muller, U.A. Kohler, S. Trzebanski, Y. Vinik, H.M. Raj, J.A. Girault, N. Ben-Chetrit, A. Maraver, S. Jung, S. Lev, Mouse modeling dissecting macrophage-breast cancer communication uncovered roles of PYK2 in macrophage recruitment and breast tumorigenesis, Adv. Sci. 9 (2022) e2105696.
[46] L. Ren, J. Yi, Y. Yang, W. Li, X. Zheng, J. Liu, S. Li, H. Yang, Y. Zhang, B. Ge, S. Zhang, W. Fu, D. Dong, G. Du, X. Wang, J. Wang, Systematic pan-cancer analysis identifies APOC1 as an immunological biomarker which regulates macrophage polarization and promotes tumor metastasis, Pharmacol. Res. 183 (2022) 106376.
[47] S. Du, J. Qian, S. Tan, W. Li, P. Liu, J. Zhao, Y. Zeng, L. Xu, Z. Wang, J. Cai, Tumor cell-derived exosomes deliver TIE2 protein to macrophages to promote angiogenesis in cervical cancer, Cancer Lett. 529 (2022) 168–179.
[48] Y. Sun, Y. Qian, C. Chen, H. Wang, X. Zhou, W. Zhai, L. Qiu, X. Zhou, H. Ning, Y. Zhao, C. Shi, L. Han, Y. Qi, Y. Wu, Y. Gao, Extracellular vesicle IL-32 promotes the M2 macrophage polarization and metastasis of esophageal squamous cell carcinoma via FAK/STAT3 pathway, J. Exp. Clin. Cancer Res. 41 (2022) 145.
[49] J. Liu, Y. Yang, Z. Liu, X. Fu, X. Cai, H. Li, L. Zhu, Y. Shen, H. Zhang, Y. Sun, H. Chen, B. Yu, R. Zhang, J. Shao, M. Zhang, Z. Li, Multicenter, single-arm, phase II trial of camrelizumab and chemotherapy as neoadjuvant treatment for locally advanced esophageal squamous cell carcinoma, J. Immunother. Cancer 10 (2022).
[50] Z. Liu, Y. Zhang, N. Ma, Y. Yang, Y. Ma, F. Wang, Y. Wang, J. Wei, H. Chen, A. Tartarone, J.B. Velotta, F. Dayyani, E. Gabriel, C.J. Wakefield, B. Kidane, C. Carbonelli, L. Long, Z. Liu, J. Su, Z. Li, Progenitor-like exhausted SPRY1(+)CD8(+) T cells potentiate responsiveness to neoadjuvant PD-1 blockade in esophageal squamous cell carcinoma, Cancer Cell (2023).